IOP Conf. Series: Materials Science and Engineering **406** (2018) 012032 doi:10.1088/1757-899X/406/1/012032

Tensile characterization of 3D nanostitched p-aramid/ phenolic MWCNTs composites

K Bilisik[1*], **G Erdogan**[1], **N S Karaduman**[2], **G Kaya**[3], **E Sapanci**[4], **S Gungor**[4]

[1]Nano/Micro Fiber Preform Design and Composite Lab., Faculty of Engineering, Erciyes University, 38039 Talas-Kayseri, Turkey
[2]Akdagmadeni Vocational High School, Bozok University, 66300 Akdagmadeni-Yozgat, Turkey
[3]Department of Textile Engineering, Faculty of Engineering and Architecture, Kahramanmaras Sutcu Imam University, Kahramanmaras, Turkey
[4]Advanced Material Development Unit, ROKETSAN Industries, 06780, Elmadag-Ankara, Turkey

* kadirbilisik@gmail.com

Abstract. The tensile properties of nanostitched and nanoprepreg three dimensional para-aramid/phenolic composites were studied. The tensile responses of para-aramid/phenolic composites showed three regions as initial inter-fiber friction, crimp exchange and yarn extension regions. Their tensile moduli in each region were defined. It was obtained that stitching and multiwall carbon nanotubes slightly increased the tensile strength of all stitched and stitched/nano composites. Tensile failure on all stitched structure showed brittle matrix and multiple ductile filament breakages in yarn after angular deformation in composite surface layers as well as local restricted delamination. Failure mechanism of carbon stitched composite was interestingly different compared to para-aramid stitched composite in where carbon stitching yarn was failed in the loop section. It was pulled out thickness direction of the composite and caused large local opening between layers.

1. Introduction

Nano/Micro filament preform composites are used in various fields such as aviation/aerospace, ballistics and civil engineering because of their high specific properties and exceptional damage tolerance behaviour [1, 2]. Z-directional reinforcement can be incorporated to textile preforms by using three-dimensional (3D) weaving, 3D braiding [4], and through-the-thickness stitching [5, 6]. In addition to these methods, recent studies have focused on the use of nanomaterials such as nanospheres, nanotubes, nano graphane platelets and nanofibers to obtain z-reinforcement. Techniques such as shear mixing, ultrasonication and transfer-printing have been used to disperse the nanomaterial in the resin [7, 8]. 3D textile reinforced composites generally exhibit low in-plane properties due to the presence of z-fibers which reduce the in-plane fiber volume fraction ratio. Nanomaterials incorporated in the composite structure, on the other hand, usually fail to provide an effective z-directional reinforcement because they generally have a discontinuous form and a random distribution rather than aligning in the thickness direction. In-plane tensile and impact strengths as well as flexural properties increased because of homogeneous topological arrangements of stitching fibers [9, 10].

Several studies have reported improvements in composite properties when nanomaterials are used in the structure. Tensile properties increased when multiwalled carbon nanotubes (MWCNTs) were used [11]. Incorporation of nanoclay enhanced the E-glass/vinyl ester composites [12, 13]. An increased amount of nanosilica from 2.5% to 7.5% significantly enhanced the principal and off-axis tensile properties of the E-glass/polyester composites [14]. Stitching also slightly increased the tensile characteristics of the E-glass/polyester nanosilica composites when compared to unstitched samples [15]. The damage was confined to a smaller area in stitched E-glass/polyester nanosilica composites [14, 15]. Composites reinforced with CNTs-coated carbon fibers displayed approximately 66% higher tensile strength compared with that of the base sample [16]. Addition of coated nanotubes noticeably improved the interface properties of the E-glass/vinyl ester composites [17]. Silane modification led to a more homogeneous dispersion of MWCNTs in epoxy matrix [18]. Amino functionalized carbon nanofibers (A-CNF, 1%) can considerably improve the in-plane mechanical strength of the laminated carbon/epoxy composite [19].

In this study, the tensile properties of stitched and MWCNTs-added para-aramid/phenolic composites were investigated.

2. Materials and methods

2.1. Nanostitched para-aramid/phenolic nanoprepreg based 3D nanopreform and composite

Para-aramid Twaron® basket (2/2) fabrics (CT736, Teijin, JP) with an areal density of 410 g/m^2 and warp/weft densities of 127 ends/cm were used to fabricate multistitched 3D nanopreform. The fabric was formed from 168 tex fibers and the fabric thickness was 0.62 mm. The average crimp of p-aramid fabrics was 10.35 % for basket (2/2). MWCNTs (Nanothinx, GR) used in this study were 15-35 nm in diameter, 10 μm in length and 1-2 nm in wall thickness. Their purity ratio was over 97%. Their average tensile strength and modulus values were 200 GPa and 1 TPa, respectively [20].

Principally, four types of p-aramid structures were developed: a) base (TBU), which was made up of six layers of Twaron basket (2/2) woven fabrics without stitch; b) stitched (TB-CS, TB-TS), the same as the base structure but the fabric layers are stitched through-the-thickness using carbon and Twaron stitching yarns. The stitches were applied in the longitudinal direction (0°) of the structure; c) base/nano (TBU-N) structures were obtained by adding MWCNTs to the base structures; d) stitched/nano (TB-CS-N, TB-TS-N) samples were obtained by adding MWCNTs to the stitched structures. Stitching was performed manually in the longitudinal direction of the structures using PAN based carbon and Twaron CT stitch yarns. The nanostitched and nanoprepreg composite samples are shown in figure 1. The stitch yarn properties are given in table 1. The preforms were consolidated via compression molding to obtain composite samples. The processing details for the mixing of the phenolic resin (Araldite EPN 1138, Biesterfeld Spezialchemie GmbH, DE) with MWCNTs and for the composite production were given in reference [21] and we would like not to repeat the processing steps and readers are advised to look through the above-mentioned reference.

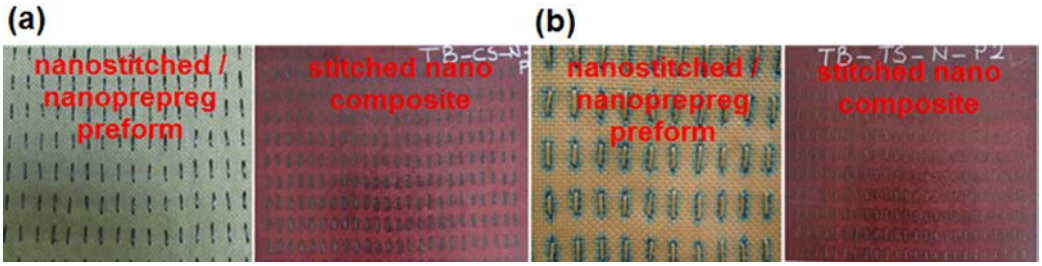

Figure 1. (a) PAN carbon multistitched 3D nanoprepreg preform (left) and p-aramid/phenolic MWCNT composite (right) (TB-CS-N); (b) para-aramid Twaron CT multistitched 3D nanoprepreg preform (left) and p-aramid/phenolic MWCNT composite (right) (TB-TS-N).

Table 1. Specifications of untwisted stitching yarns.

Fiber type	Tensile strength (GPa)	Tensile modulus (GPa)	Elongation at break (%)	Yarn linear density (dtex)
Twaron CT (Para-aramid fiber, Teijin, JP)	3.2	115	2.9	3360
Polyacrylonitrile (PAN) carbon (Carbon fiber, Aksaca, TR)	4.2	240	1.8	6 K[1]

2.2. Tensile test

The tensile tests of the composite samples were performed according to ASTM D3039-14 standard [22] on a Shimadzu AG-XD (JP) tester with a 5kN loading cell and equipped with Trapezium® data acquisition software (figure 2). The crosshead speed was 2 mm/min and the load was applied in the longitudinal (warp) direction of the structures. The tensile characteristics of the composite samples were calculated according to Eqs. 1-4.

$$F = P / A \quad (1)$$

$$\sigma_i = P_i / A \quad (2)$$

$$\varepsilon_i = \delta_i / L_g \quad (3)$$

$$E = \Delta\sigma / \Delta\varepsilon \quad (4)$$

Where F is the ultimate tensile strength (MPa), P is the maximum force before failure (N), A is the average cross-sectional area (mm^2), σ_i is the tensile stress at ith data point (MPa), P_i is the force at ith data point (N), ε_i is the tensile strain at ith data point, δ_i is the extensometer displacement at ith data point (mm), L_g is the extensometer gage length (mm), E is the tensile modulus of elasticity (GPa), $\Delta\sigma$ is the difference in applied tensile stress between the two stain points (MPa) and $\Delta\varepsilon$ is the difference between the two strain points.

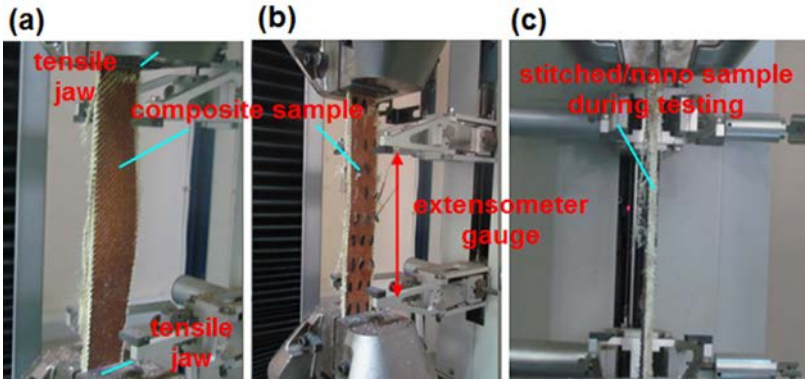

Figure 2. Tensile testing instrument with sample. (a) p-aramid/phenolic/MWCNT composite (TBU-N); (b) carbon multistitched p-aramid/phenolic composite (TB-CS); (c) p-aramid multistitched p-aramid/phenolic/MWCNT composite (TB-CS-N, digital image).

3. Results and discussion

3.1. Tensile results

The tensile test data of base (TBU), stitched (TB-CS, TB-TS), base/nano (TBU-N) and stitched/nano (TB-CS-N, TB-TS-N) composites are generated. Figure 3 shows the tensile stress-strain curves of some of the basket (2/2) fabric composites.

In figure 3, the tensile properties of stitched and stitched/nano composites were found to be generally higher compared with unstitched composites. Tensile stress-strain curves of the tested samples showed three distinct stages such as the inter-fiber friction, crimp exchange and yarn extension. In the first stage, yarn-yarn friction and micro shear took place. In the crimp exchange stage, warp crimp was removed leading to a large fabric extension. In the final i.e. yarn extension stage, the uncrimped yarns were strained to the point of final failure.

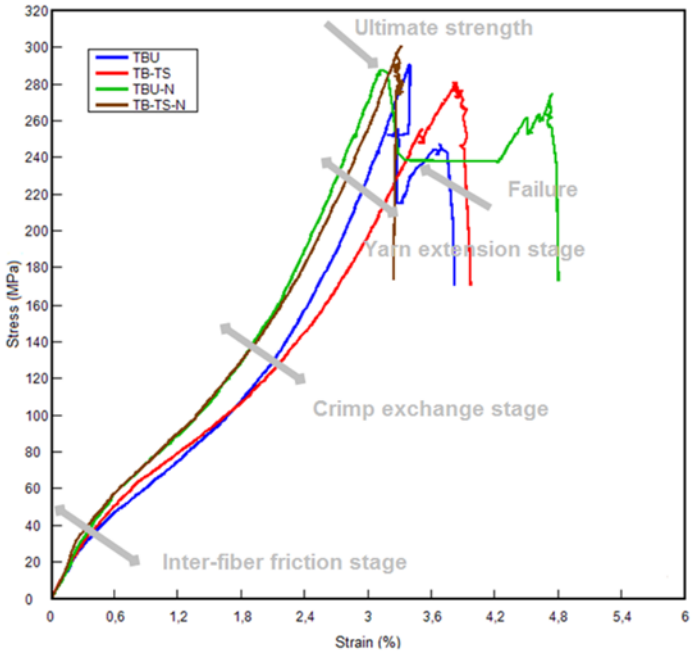

Figure 3. Stress-strain curves from tensile test for some of the multistitched p-aramid/phenolic MWCNT composites (based TBU, stitched TB-TS, base/nano TBU-N, stitched/nano TB-TS-N) [21].

3.2. Tensile strength

The tensile strength values of the developed structures are presented in figure 4. Stitched and stitched/nano structures generally displayed greater strength values (up to 7.73%) over the unstitched ones. There is no significant difference between the strength values of the stitched and stitched/nano composites and it is reasonable to state that the nanomaterial had only limited effect on the tensile properties. Stitching and nano addition slightly increased the strain values of the composites (up to 6.08%). The average tensile strain values were almost the same for the base and base/nano structures. However, the strain value of the stitched/nano sample was about 2.48% higher compared with that of the stitched structure.

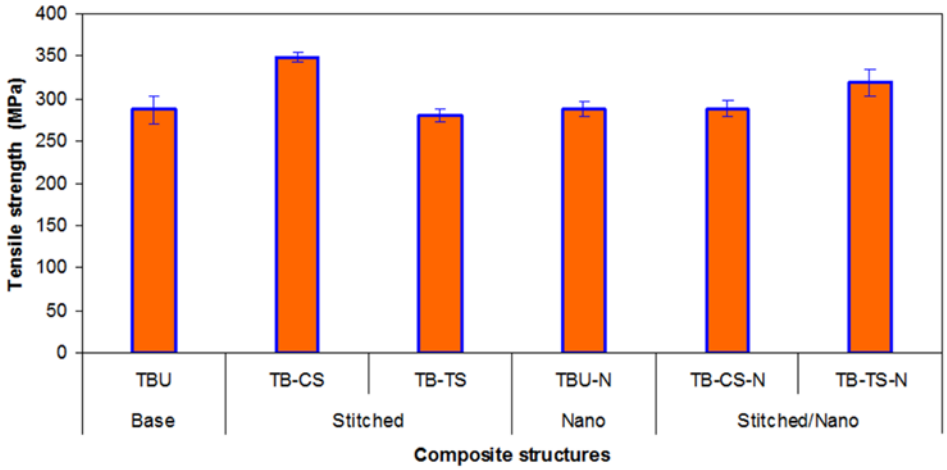

Figure 4. Tensile strength of various developed p-aramid/phenolic MWCNT composites.

3.3. Tensile modulus

The average tensile modulus values are shown in figure 5. Three different modulus values were calculated each corresponding to the three distinct load-elongation stages on the stress-strain curves (figure 3). The modulus of inter-fiber friction stage (E_{ff}) was calculated from the initial straight portion of the stress-strain curve and was relatively high due possibly to friction between fibers and the surrounding matrix. The modulus of crimp exchange stage (E_{ce}) was calculated from the following non-linear portion of the curve and it was relatively lower because of crimp extension at this stage. The final stage involved yarn extension in the form of tensile elongation of the yarns. The modulus at this stage was defined as the modulus of yarn extension stage (E_{ye}) and is higher compared with the E_{ce} due to decreased crimp ratio and to the fact that the extension took place as tensile elongation of low-twisted Twaron yarns (1-2 twist/meter).

As illustrated in figure 5, it was found that the E_{ff} was higher than the E_{ce} and E_{ye} due to initial inter-fiber friction stage of the stress-strain curve. The E_{ye} was also higher than the E_{ce} because of high extension in the crimp interchange stage of the composite. The average E_{ff} of all stitched composites was 7.20% higher than that of all base structures. Additionally, the E_{ff} of all base/nano composites were almost the same compared to all base structures. On the other hand, the E_{ff} of all stitched composites were slightly higher (18%) than the stitched/nano composites. It was realized that the stitching slightly increased the E_{ff} of all stitched composites. The E_{ce} and E_{ye} of all developed composites were almost near to each other.

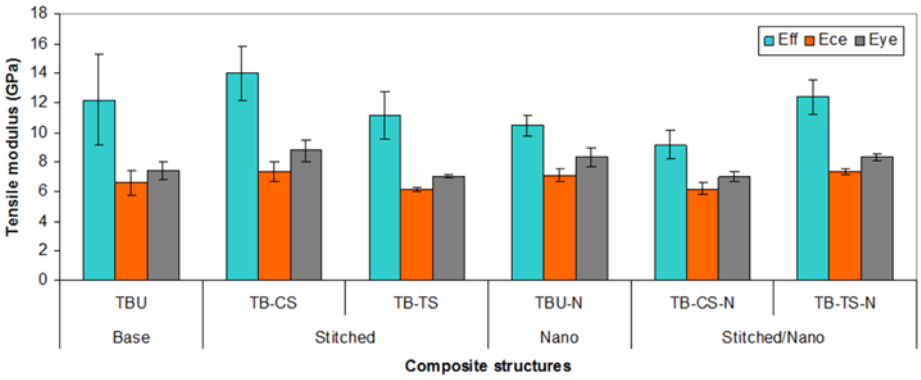

Figure 5. Tensile modulus of various developed p-aramid/phenolic MWCNT composites.

3.4. Failure characterization after tensile test

The post-tensile fracture characterization of the developed structures was performed. Figure 6 (a-c) presents the post-tensile failure pictures of base/nano (TBU-N) and stitched/nano (TB-TS-N, TB-CS-N) samples. TBU and TBU-N samples were subject to warp and lateral yarn splitting at the edge of the specimen as well as fiber and matrix failures due to the tensile load. Large delamination areas were also observed in these specimens (Figure 6 (a)). With regards to the stitched and stitched/nano structures i.e. TB-TS and TB-TS-N samples, delamination was largely constrained to smaller areas due to the stitch yarns. The failure mode of this specimen also involved warp yarn splitting, stitch yarn failure, warp/filling yarn breakages and matrix cracking as well as shear failures (Figure 6 (b)).

With regards to the carbon-stitched structures, i.e. TB-CS and TB-CS-N, fiber breakages and matrix cracking were the dominant failure mode whereas failure due to shear load was also observed. The carbon stitch yarn failed at the stitch loop section and pulled out of the lamina layers in thickness direction causing local delamination of the layers (Figure 6 (c)). It can be concluded that the stitch yarn largely limited the extent of delamination and reduced the total damage area when compared to the unstitched samples.

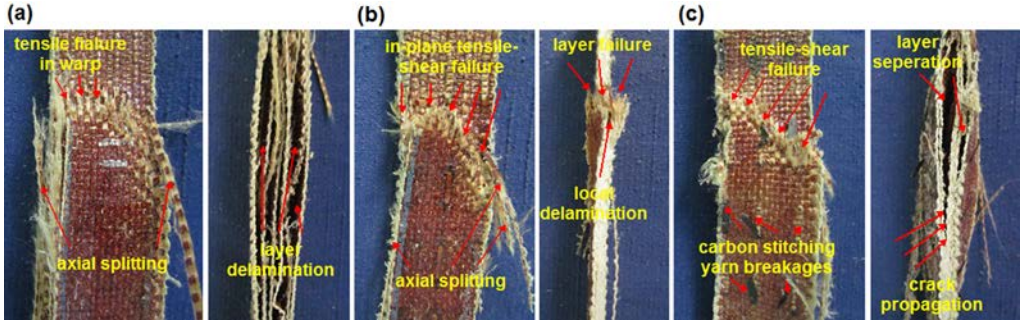

Figure 6. Warp directional top and side view (thickness) of tensile failure in various multistitched 3D p-aramid/phenolic MWCNT composites. (a) base/nano (TBU-N); (b) basket 2/2 p-aramid stitched/nano (TB-TS-N); (c) basket 2/2 carbon stitched/nano (TB-CS-N) (optical microscope, magnification x6.7) [21].

Figure 7 (a-b) shows the SEM photomicrographs of the failed samples TB-TS and TB-TS-N. TB-TS sample was subjected to multiple warp yarn failures on the top layer. Closer inspection of the failed region suggests warp yarn splitting and warps breakages (figure 7 (a)). Ductile multiple yarn end failure in the front face of the TB-TS-N structure was identified. Some of the failed filament has axial splitting probably due to weak cross bonding in the out-of-plane direction as exhibited in figure 7 (b).

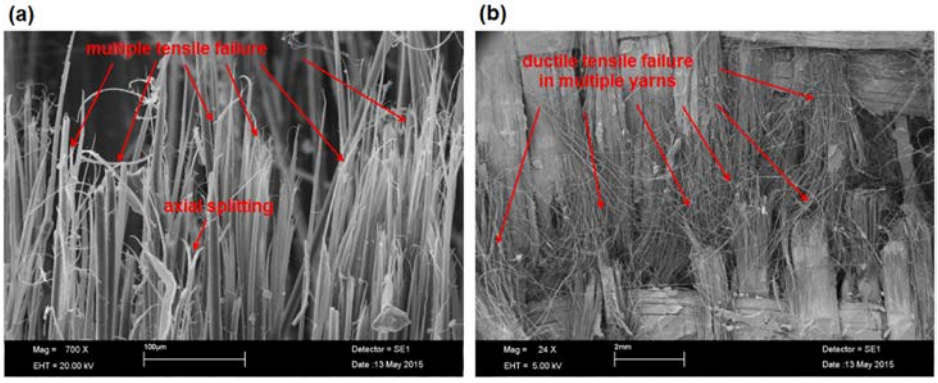

Figure 7. (a) SEM (LEO 440® model, UK) views of failed p-aramid stitching yarn filaments (TB-TS); (b) broken p-aramid stitching nano prepreg yarn in the delaminated failed surface of p-aramid/phenolic MWCNT composite (TB-TS-N) [21].

5. Conclusions

Tensile properties and failure pattern of the stitched and stitched/nano p-aramid composites were investigated. Stress-strain profile of the developed structures involved three different stages such as inter-fiber friction, crimp exchange and yarn extension. The modulus value in inter-fiber friction region was higher compared to those in the crimp exchange and yarn extension regions due to friction to the yarn in the matrix. Tensile strength and strain generally increased as a consequence of stitching and nanomaterial addition. The modulus value in inter-fiber friction region was slightly higher in stitched composites compared with that of the unstitched samples whereas other two moduli i.e. crimp exchange and yarn extensions were almost the same for all structures.

Ductile warp and weft yarn failures and matrix cracking were the primary failure mode in the structures. Para-aramid stitch yarn successfully constrained the layer-to-layer delamination in the samples whereas carbon stitch yarn failed at the stitch loop region and was pulled out of the structure in the thickness direction resulting in large delamination. It can be noted that the stitch yarn largely limited the extent of delamination and reduced the total damage area when compared to the unstitched samples. These results showed that stitching and multiwalled carbon nanotube addition improved the in-plane properties of the resulting p-aramid based composites.

Acknowledgements

This work was supported by Roketsan Industries Grant No. RS/ERCİYES DSM-76301-14-01N/R. The authors would like to thank Erciyes University Technology Research and Application Center (ERÜ TAUM) for tensile tests.

References

[1] Dow M B and Dexter H B 1997 Development of stitched, braided and woven composite structures *ACT Program at Langley Research Centre* NASA/TP-97-206234.
[2] Kamiya R, Cheeseman B A, Popper P and Chou T W 2000 *Compos. Sci. Technol.* **60** 33-47.
[3] Bilisik K 2012 *Text. Res. J.* **82** 725-743.
[4] Bilisik K 2013 *Text. Res. J.* **83** 1414-1436.
[5] Tong L, Mouritz A P and Bannister M K 2002 *Stitched Composites* In: 3D Fibre Reinforced Polymer Composites. New York: Elsevier B.V. 163-204.
[6] Bilisik K and Yolacan G 2014 J. *Compos. Mater.* **48** 2145-2162.
[7] Garcia E J, Wardle B L and Hart A J 2008 *Compos. A* **39** 1065-1070.
[8] Khan S U and Kim J-K 2011 *Int. J. Aeronaut. Space* **12** 115-133.
[9] Velmurugan R and Solaimurugan S 2007 *Compos. Sci. Technol.* **67** 61-69.
[10] Mouritz A P 2004 *Fracture and tensile fatigue properties of stitched fibreglass composites.* In: Proceedings of the Institution of Mechanical Engineers, Part L: Journal of Materials: Design and Applications **218** 87-93.
[11] Guo P, Chen X, Gao X, Song H and Shen H 2007 *Comp. Sci. Tech.* **67** 3331-3337.
[12] Chandradass J, Kumar M R and Velmurugan R 2008 *J. of Reinf. Plast. and Compos.* **27** 1585-1601.
[13] Bozkurt E, Kaya E and Tanoglu M 2007 *Compos. Sci .Tech.* **67** 3394-3403.
[14] Bilisik K and Yolacan G 2014 *Fiber. Polym.* **15** 1051-1061.
[15] Bilisik K and Yolacan G 2014 *Fiber. Polym.* **15** 614-624.
[16] Sharma S P and Lakkad S C 2011 *Compos. A* **42** 8-15.
[17] Zhu J, Imam A, Crane R, Lozano K, Khabashesku VN and Barrera EV 2007 *Compos. Sci. Tech.* **67** 1509-1517.
[18] Fukushima T, Kosaka A, Ishimura Y, Yamamoto T, Takigawa T, Ishii N and Aida T 2003 *Science* **300** 2072-2076.
[19] Srikanth I, Kumar S, Singh V, Rangababu B, Ghosal P and Subrahmanyam H 2015 *Bull. Mater. Sci.* **38** 1-9.
[20] http://www.nanothinx.com/raw-cnts-in-powder-form/; 2017 [accessed 17.02.17].
[21] Bilisik K, Erdogan G and Sapanci E 2018 *Polym. Compos.* https://doi.org/10.1002/pc.24847.
[22] ASTM D3039-14. 2014 Standard test method for tensile properties of polymer matrix composite materials.